J. Braz. Chem. Soc., Vol. 6, No. 3, 277-285, 1995.
Printed in Brazil.

0103 – 5053 $5.00 + 0.00

New Approaches to Surface Electrochemistry

A.J. Arvia and R.C. Salvarezza

Instituto de Investigaciones Fisicoquímicas Teóricas y Aplicadas (INIFTA),
Facultad de Ciencias Exactas, Universidad Nacional de La Plata. Sucursal 4,
Casilla de Correo 16, 1900 La Plata, Argentina

Received: March 20, 1995

A topografia e outras propriedades relacionadas com superfícies metálicas desordenadas têm um papel importante nos fenômenos de deposição, corrosão e crescimento. As superfícies metálicas resultantes de depósitos metálicos colunares ou dendríticos podem ser consideradas modelos de desordem superficial anisotrópica e isotrópica, respectivamente. A topografia de superfícies colunares rugosas pode ser determinada por microscopia de tunelamento em diferentes escalas e descrita pela teoria do dimensionamento dinâmico. A cinética de relaxação da rugosidade pode ser acompanhada por técnicas eletroquímicas e interpretada por meio de um mecanismo tipo coalescência. São apresentados exemplos típicos de reações eletroquímicas sobre eletrodos com este tipo de superfície. O estudo da formação eletroquímica 3D ou 2D de metais ramificados fornece informações básicas acerca do desenvolvimento de padrões tipo agregação limitada por difusão ou tipo radial denso, a forma do depósito e as condições de trabalho. Neste caso, estabeleceu-se a influência da convecção e, particularmente, a contribuição relativa da migração e difusão para determinar a topografia do objeto. Um modelo generalizado baseado em uma simulação de Monte Carlo justifica os resultados experimentais.

The topography and other properties related to disordered metal surfaces play an important role in deposition, corrosion and growth phenomena. Metal surfaces resulting from columnar or dendritic metal deposits can be taken as models of anisotropic and isotropic strong surface disorder, respectively. The topography of rough columnar surfaces can be determined by scanning tunneling microscopy at different scales and described by means of the dynamic scaling theory. Roughness relaxation kinetics can be followed by electrochemical techniques and interpreted through a coalescence-type mechanism. Typical examples of electrochemical reactions electrodes with this surface type are presented. The study of the electrochemically formed 3D or 2D branched metal provides basic information about the development of either diffusion limiting aggregation-type or dense radial patterns, the design and the working conditions. In this case, the influence of convection, and particularly, that of the relative contribution of migration and diffusion to determine the topography of the object has been established. A generalized model based upon a Monte Carlo simulation accounts for the experimental results.

Keywords: *rough electrodes, irregular surfaces, fractal geometry, scanning tunneling microscopy*

Introduction

The surfaces of real systems and interfaces produced by contacting different phases are, except for very particular cases, irregular surfaces at all scales. Irregularities at the atomic level are extremely important in heterogeneous catalysis and electrocatalysis, as these irregularities define the electronic energy distribution at surface sites, whereas irregularities at the nano-micrometer scale play a key role in determining the accessibility of reactants to those active surface sites. Accordingly, the efficiency of a catalyst/electrocatalyst (substrate) for a particular reaction results from a compromise between the quality and the quantity of reaction sites. This compromise depends to some extent on the topography of the substrate. This means that among the interesting questions related to those systems, the study of the irregularity of surfaces should address those irregularities at the atomic level, a geometrical description of the surface, the kinetics of surface formation and relaxation processes leading to active surface loss, the accessibility of

the surface according to a cross section of the reactant particles, and specific properties of the surface for each reaction.

Irregularities at the Atomic Level

The use of crystallographically well-defined solid surfaces in experimental studies has contributed considerably to the advance in the knowledge of the influence of the solid surface structure on the kinetics and mechanisms of heterogeneous reactions, including surface electrochemical reactions[1]. The application of nanoscopies to the study of single crystal surfaces, at room temperature, reveals that the atomic corrugation which should be expected for a "perfectly smooth surface" is restricted to rather small surface domains (Fig. 1a). This limitation results from the existence of structural defects at real single crystal surfaces, such as steps, kinks, vacancies, clusters of atoms, etc. (Fig. 1b), and chemical defects resulting from the presence of adsorbates at the submonolayer level (Fig. 1c). All this implies the existence of an atomic level roughness in well-defined solid surfaces[2,3].

The high mobility of a number of metal surface atoms at room temperature favors surface restructuring phenomena. Restructuring can also be induced or promoted by adsorbates[3]. Hence, at a single crystal surface, the coexistence of reconstructed and unreconstructed domains may result in a solid surface with an appreciable degree of heterogeneity. Metallic surfaces of this type can be produced by electrochemical faceting applied to single crystal electrodes in acid solution[4].

From the above description, real single crystal surfaces immersed in aqueous electrolytes must be considered as weakly disordered, as they involve a certain degree of surface irregularity. This fact is particularly relevant in dealing with the kinetics and mechanisms of electrocatalytic reactions.

Geometric Description of Irregular Solid Surfaces

In general, from the standpoint of heterogeneous reactions, the irregular surface of solids in contact with a fluid can be continuous or discontinuos. A continuous solid surface implies a homogeneous phase such as, for instance, a metal surface. Otherwise, a discontinuous solid surface involves a solid formed by two different phases as occurs for a solid catalyst involving an active material dispersed in a substrate.

On the basis of a continuous geometric model[5] the surface of a continuous solid phase can be described as ordered (smooth), weakly disordered (stepped or reconstructed), or strongly disordered. This description can be extended to a discontinuous solid surface as a whole or to domains formed by each constituent.

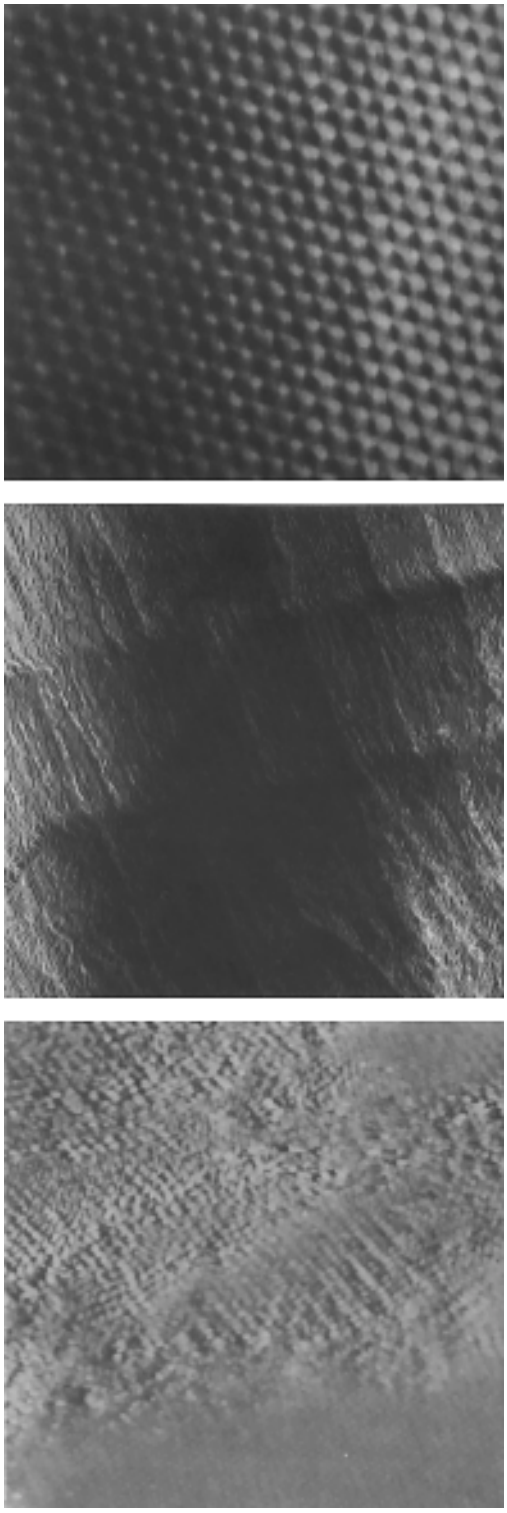

Figure 1. STM images. a) Highly oriented pyrolitic graphite (HOPG) basal plane. A domain 4 x 4 nm^2 in size. Atomic resolution of the hexagonal structure can be observed. b) Pt(111) surface 300 x 300 nm^2 in size. Steps of different heights from a single step height upwards can be seen. c) A HOPG domain15 x 15 nm^2 in size, partially covered by sulphur atoms. The upper part exhibits a structural disorder caused by the presence of adsorbate.

Strongly disordered surfaces

Strongly disordered surfaces can be anisotropically disordered, when the disorder extends in two space directions only, as occurs in rough surfaces (Fig. 2a), or isotropically disordered in space such as, for instance, in dendrite surfaces (Fig. 2b).

A more realistic description of strongly disordered surfaces can perhaps be given in terms of fractal instead of conventional euclidean geometry. The fractal approach to studying irregular surfaces offers, for the first time, the possibility of getting qualitative and quantitative information about the degree of disorder at irregular surfaces. Likewise, this approach allows a more realistic interpretation of both the kinetics of irregular surface formation and physicochemical processes taking place at those surfaces[5,6]. Recent advances have led to the development of new methods for the characterization of irregular solid surfaces and to more convincing explanations of some "anomalous" kinetic behavior resulting from adsorption interactions and heterogeneous chemical reactions on large area irregular surfaces[7].

Anisotropic disorder. Rough solid surfaces

A rough solid surface can be described as an irregular, overhang-free surface, *i.e.*, if overhangs are present they do not dominate the scaling properties of the surface[8]. Consequently, rough surfaces are irregular anisotropic surfaces, and according to fractal geometry, these surfaces can be considered as self-affine fractals[6]. The simplest model of a rough surface is the solid-on-solid (SOS) model[8].

A rough surface can be produced either by the addition of material for the growth of the new phase or by the removal of material from an initially smooth surface[8]. In any case, the aggregation or desintegration which yields rough surfaces is favored at relatively high rates and low temperatures at which the surface atom mobility decreases considerably. Images of the rough surfaces of vapor-deposited gold film on a smooth glass plate (Fig. 3a), electrode-

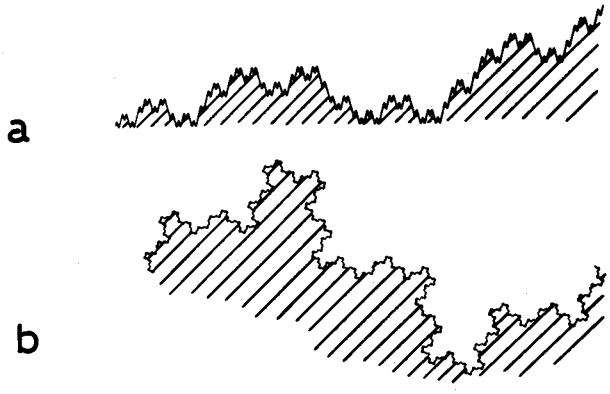

Figure 2. Irregular surface profiles. a) Anisotropic disorder. b) Isotropic disorder.

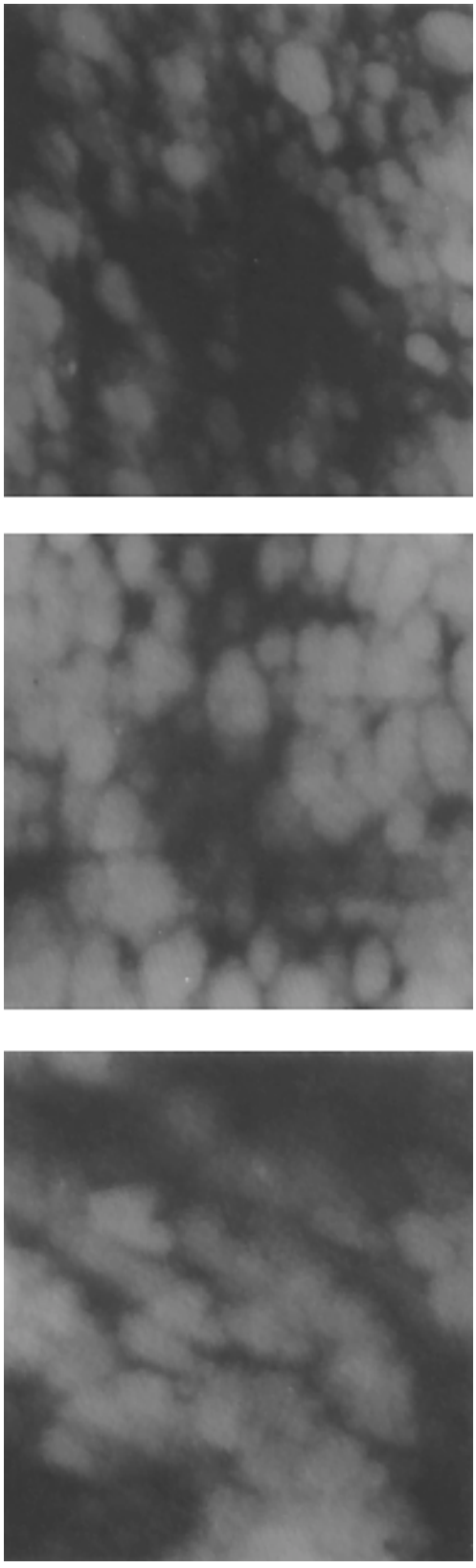

Figure 3. STM images. a) Vapor-deposited gold on glass, 300 x 300 nm^2. b) Electrodeposited gold on a gold cathode, 300 x 300 nm^2. c) Poly-o-toluidine film deposited on a gold single crystal, 250 x 250 nm^2.

posited gold film on gold (Fig. 3b), and a conducting polymer film produced electrochemically on gold (Fig. 3c), which have been produced at a high deposition rate are shown in Fig. 3. These images exhibit a common topography, independent of the substrate, which consists of rounded elements randomly distributed in size and height leading to an irregular topography. It would appear that the topography of the different deposits evolves spontaneously towards a unique standard surface. This standard surface under a quasi-steady regime is characterized by universal self-affine fractal properties[9].

The dynamic scaling theory

The dynamic scaling theory[10] appears to be a very convenient tool for describing self-affine fractal surfaces such as rough solid surfaces. This theory makes it possible to obtain quantitative information about rough surface properties under the quasi-steady regime, as well as kinetic data about roughness growth kinetics.

The simplest form of the dynamic scaling theory considers the development of a bidimensional surface profile resulting from material aggregation onto an initially (t = 0) smooth surface (substrate). The length of the substrate is L. The height of the bidimensional deposit, h, develops exclusively in the direction perpendicular to L, without overhangs. As such, the instantaneous height of the deposit can be described by the function h(x,t) where x is a coordinate along L. The interface width, ξ(L,t), can be taken to measure the surface roughness at time t. The term ξ(L,t) corresponds to the standard deviation of height fluctuations[8], *i.e.*,

$$\xi(L, t) = [1/L \sum [h(x_i) - \langle h \rangle]^2]^{1/2} \quad (1)$$

where h is the average height of the deposit in the direction of growth. The dependence of ξ(L,t) on L and t is given by the proportionality

$$\xi(L, t) \propto L^{\alpha} f(x) \quad (2)$$

with $x = t/L^{\alpha/\beta}$, f(x) = constant for $x \rightarrow \xi$, and $f(x) = x^{\beta}$ for $x \rightarrow 0$. Thus, initially, the value of ξ increases with t according to

$$\xi(L, t \rightarrow 0) \propto t^{\beta} \quad (3)$$

where the exponent β describes the kinetics of roughness development in the direction of the growth of the deposit.

After a certain growth time or an average deposit thickness coinciding with h, the value of ξ(L,t) attains a quasi-steady regime, and the following expression results

$$\xi(L, t \rightarrow \infty) = L^{\alpha} \quad (4)$$

The surface of the deposit in the quasi-steady regime becomes a self-affine fractal, independent of the scale length. Furthermore, exponent α quantitatively describes the roughness properties of the system[8,9].

On the other hand, exponent α is related to the local fractal dimension, D_s, of the rough surface by the expression

$$D_s = d - \alpha \quad (5)$$

where d is the dimension of the growing space. Small values of α are related to a sawtooth profile (anti-correlation), whereas high values of α correspond to smooth texture surfaces (correlation) (Fig. 4). In addition, the value of D_s provides information about the degree of surface disorder, the mechanism of roughness development and the reactivity of the rough surface.

Experimental methods for the characterization of rough surfaces

The fractal behavior of real systems is obeyed in a certain scale range (cutoffs). For thin metallic layers the cutoffs are in the nanometer range. This is one important reason why scanning tunneling microscopy (STM) and atomic force microscopy (AFM) are important tools for rough surface characterization. These techniques offer a high lateral resolution and the possibility of tridimensional imaging in real space. In addition, they provide complete topographic information in the absence of overhangs.

The dynamic scaling theory is adequate for the characterization of rough surfaces and, as is discussed elsewhere[11], the theory can be straightforwardly applied to STM imaging by considering $\xi = \xi^i_{STM}$, where ξ^i_{STM} is the standard deviation of heights resulting from STM image profiles in the i-direction (i = x,y). Explicitly, the following proportionality is used

$$\xi^{i}_{STM}(L_s) \propto [1/L_s \sum [h(x_i - \langle h_s \rangle)]^2]^{1/2} \quad (6)$$

where $\langle h_s \rangle$ is the average height of the deposit profile of length L_s, resulting from the STM image in the i-direction.

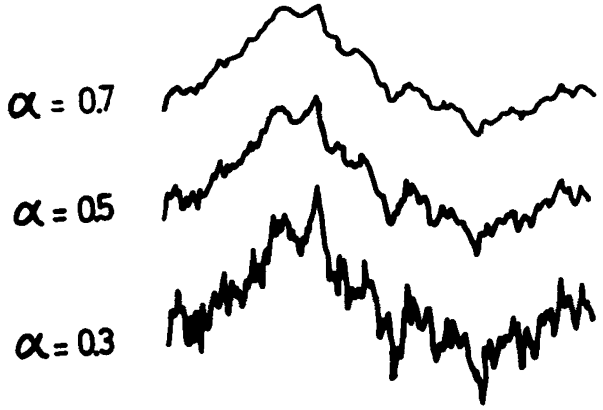

Figure 4. Self-affine profiles with different α values.

Considering that in those aggregation processes under surface reaction control, the value of h is directly proportional to the growing time, $\langle h \rangle \rightarrow 0$, and the value of exponent β can be calculated from the proportionality

$$\xi^{i}_{STM} \propto \langle h \rangle^{\beta} \quad (7)$$

On the other hand, once the steady-state regime is attained, *i.e.*, when ξ^{i}_{STM} becomes independent of $\langle h \rangle$, the value of exponent α can be estimated from the relationship

$$\xi^{i}_{STM} \propto L_s^{\alpha} \quad (8)$$

The suitability of the calculation procedure outlined above has been demonstrated by applying it to a number of self-affine fractal surfaces with known values of α generated by a random sum algorithm[12].

It was then shown that for 250 x 250 pixel files such as those usually employed to store STM images, the calculation procedure underestimates the value of α when $\alpha > 0.5$[13]. The difference between α, the calculated α value, and α_{th}, the expected α value, decreases progressively as the file size is increased, for instance, to 400 x 400, 512 x 512 or 1000 x 1000 pixels. However, it should be noted that file sizes greater than 256 x 256 pixels require a much longer acquisition time, and therefore, the influence of the piezo's shift on STM due to the thermal effect results in a greater possibility of image distortion. As such, with the present STM facilities, this drawback can be solved using 256 x 256 pixel images and data derived from these images corrected from a α *vs.* α_{th} plot. This correction becomes negligible when the analysis of data is made from 512 x 512 pixel STM images.

The above-mentioned procedure was applied to the quantitative characterization of rough gold deposits grown on a smooth plane glass substrate. These deposits offer a columnar structure with a preferred (111) crystallographic orientation[13,14]. The voltammogram of these deposits in aqueous sulphuric acid, at room temperature, tends to be similar to that resulting from gold (111) in the same solution.

The profile evolution of rough gold deposits followed by STM imaging shows that as $\langle h \rangle$ increases, random fluctuations are due to the competitive growth of columns averaging 30 nm in size. For each deposit the value of ξ_{STM} increases with $\langle h \rangle$ and time (Fig. 5) until the quasi-steady regime is attained for $\langle h \rangle > 500$ nm. For $\langle h \rangle > 500$ nm, the value of α can be obtained by applying Eq. 8. In fact, for rough gold deposits the log ξ^{i}_{STM} *vs.* log L_s plot (Fig. 6), which results from the analysis of STM profiles along the fast scanning x-direction, shows two linear regions in the range 500 nm $\leq \langle h \rangle \leq$ 850 nm, with a crossing point for log $\xi^{x}_{STM} = 0.3$ and log $L_{sc} = 1.6$, and a saturation region

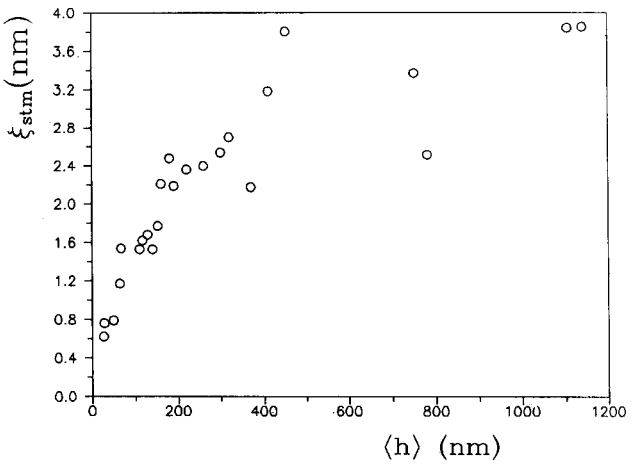

Figure 5. Dependence of ξ_{STM} on $\langle h \rangle$.

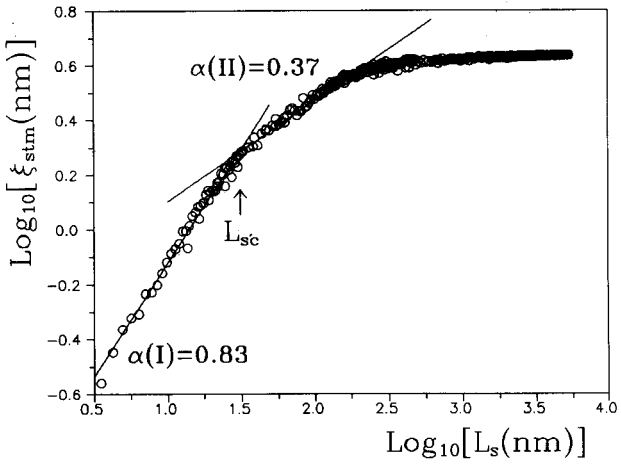

Figure 6. Plot of log ξ_{STM} *vs.* log L_s. The crossing point L_{sc} coincides with the average cross-section of columns.

for log $L_s > 2.6$. The slopes of the straight line portions are 0.83 ± 0.1 for log $L_s < 1.6$ and 0.37 ± 0.06 for $1.6 \leq$ log $L_s \leq 2.6$. The evaluation of α made from STM profiles along the slow scanning y-direction yields the same results, although they are appreciably influenced by the piezo's shift and noise produced by low frequency mechanical vibrations[13,14].

The average value of α resulting from the analysis of a large number of gold deposit STM images, for the average thickness mentioned above, is $\alpha(I) = 0.90 \pm 0.05$ for log $L_s < 1.6$ and $\alpha(II) = 0.36 \pm 0.05$ for log $L_s > 1.6$. The value $L_{sc} = 38$ nm coincides with the average columnar size resulting from the STM images.

On the other hand, the value of exponent β can be derived from Eq. 7 through a log ξ^{x}_{STM} *vs.* log $\langle h \rangle$ plot, for $\langle h \rangle < 400$ nm (Fig. 7) as required by Eq. 7. For gold deposits this plot leads to a linear relationship with the slope $\beta(I) = 0.22 \pm 0.06$ for the range $L_s < 38$ nm, and $\beta(II) = 0.45 \pm 0.06$ for $L_s < 38$ nm[15].

The values $\alpha(I) = 0.90 \pm 0.05$ and $\beta(I) = 0.22 \pm 0.06$ resulting from $L_s < 38$ nm are close to the values $\alpha = 1$, $\beta = 0.20$[16] and $\alpha = 0.66$, $\beta = 0.25$[17] resulting from 3D-growth models including surface diffusion. Otherwise, the values $\alpha(II) = 0.36 \pm 0.05$ and $\beta(II) = 0.45 \pm 0.06$ for $L_s > 38$ nm do not fit the expected $[\alpha + (\alpha/\beta)] = 2$ predicted by the Kardar, Parisi and Zhang growth model[18].

The above mentioned results allow us to conclude that the properties of the surface deposit depend on the scaling length. Thus, when the scaling length is within the average column size it results in $D_s \approx 2.1$, and roughness is then dominated by the actual mobility of gold surface atoms. Otherwise, when scaling proceeds with a length greater than the average column size, it results in $D_s \approx 2.6$, and, in this case, roughness is determined by height fluctuations produced by the columnar growth itself.

The dynamic scaling theory has also been extended to the analysis of STM profiles of other systems such as gold electrodeposits built up by the electroreduction of thick gold oxide layers with a high water content[19], conducting polymer films[20], and metal surfaces resulting from corrosion processes[21]. In all cases, the values of α and D_s were obtained (Table 1) and the self-affine character of those surfaces was confirmed.

Dynamic aspects of rough surfaces

The influence of surface diffusion on roughness development and decay was studied for vapor-deposited gold layers immersed in aqueous sulphuric acid at room temperature, both in the presence and absence of sodium chloride[22]. In the former case, after a 24 h immersion, only a slight change in $\alpha(II)$ from 0.40 to 0.43 (Table 2) was observed, whereas in the latter the value of $\alpha(II)$ was changed from 0.40 to 0.56 as the sodium chloride concentration in the solution was increased. This variation in the value of $\alpha(II)$ was accompanied by a change in the structure of the deposit from columnar to faceted. The faceted structure was similar to that resulting from vapor-deposited gold on the same substrate heated at high temperature (Fig. 8)[23].

The preceding results indicate that the surface mobility of gold atoms depends strongly on the adsorbability of ions present in the solution. Thus, chloride ions which specifically adsorb on gold induce a strong restructuring of the metal surface, in contrast to sulphate/bisulphate ions which interact more weakly with the gold surface. Accordingly, there is a correlation among the change in the value of α, the degree of restructuring, and the adsorbability of anions on the gold surface.

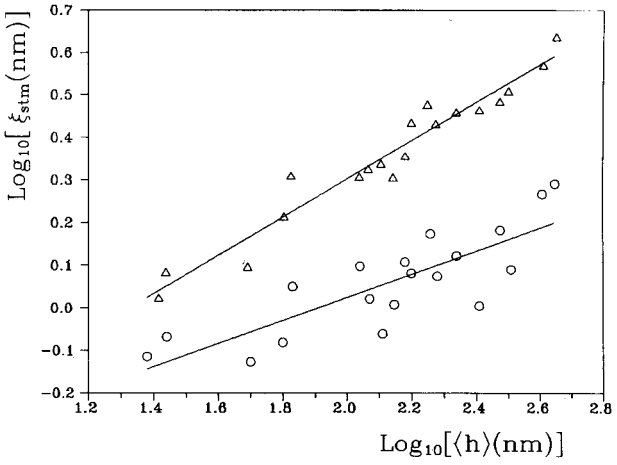

Figure 7. Plot of log ξ_{STM} *vs.* log <h>. (Δ) $L_s > 38$ nm; (O) $L_s < 38$ nm.

Table 1. Values of α and L_{sc} resulting from different rough surface systems.

System	α(I)	α(II)	L_{sc}
electrodeposited gold	0.90	0.50	$L_{sc} \propto \langle h \rangle^{1/4}$
conducting polymer	0.85	0.33	20 nm
brass de-alloyed in 0.5 M NaCl	0.8-0.7	–	–

Table 2. Values of α for vapor-deposited gold on glass at different substrate temperatures (T), after immersion in different aqueous solutions at temperature, T_c.

T K	Aqueous Solution	T_c K	α(I)	α(II)
298	none	–	0.92 ± 0.07	0.40 ± 0.05
298	H_2SO_4	323	0.90 ± 0.07	0.43 ± 0.04
298	H_2SO_4 + 0.01 M KCl	323	0.90 ± 0.07	0.49 ± 0.06
298	H_2SO_4 + 0.5 M KCl	323	0.88 ± 0.07	0.56 ± 0.06
673	none	–	0.93 ± 0.07	–

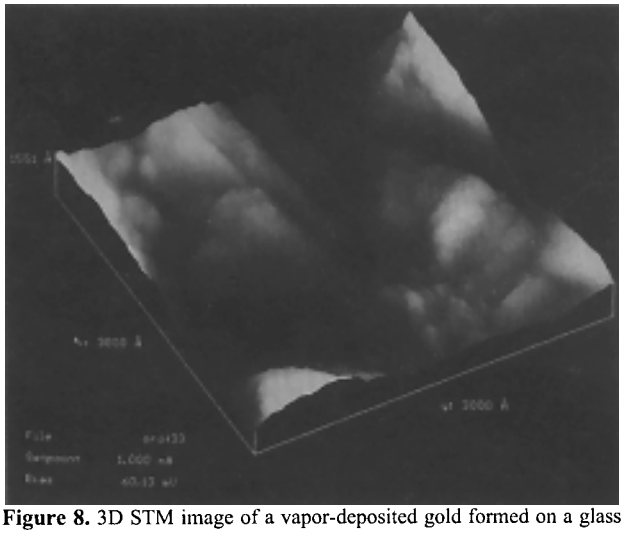

Figure 8. 3D STM image of a vapor-deposited gold formed on a glass substrate heated to 400 °C.

Comparable experiments were made with rough platinum electrodeposits in aqueous sulphuric acid[24]. These experiments demonstrate that the stability of these rough surfaces is due to the low mobility of surface platinum atoms, in contrast to that of rough gold electrodes.

Electrochemical behavior of rough metal surfaces

The impedance diagram of rough metal electrodes behaves as an anomalous diagram as compared to that resulting from smooth metal surfaces. The impedance diagram is described by the equation[25]:

$$Z(\omega) = A(i\omega)^{-s} \tag{9}$$

where A is a frequency independent parameter, $i = (-1)^{1/2}$, ω is the angular velocity ($\omega = 2\pi f$), f is the frequency, and $0 \leq s \leq 1$. In the absence of faradaic processes, $Z(\omega) = (i\omega C)^{-1}$, where C is the capacitance. Exponent s can be determined from a log ωC *vs.* log ω plot. For a smooth surface 1 = 1, whereas for a fractal surface $s < 1$[26].

The values of s which have been estimated for columnar gold deposits immersed in M H_2SO_4 and w > 2.5 kHz, are in the range of 0.70-0.75, as is expected for a fractal surface. Nevertheless, at present there is no convincing relationship between s and the fractal dimension of the surface. The frequency dispersion formed for rough deposits could be assigned to small intercolumnar pores < 10 nm in radius or thereabouts, and with a depth on the order of the deposit thickness[27].

The kinetics of a redox electrochemical reaction under diffusion control taking place at a fractal electrode also exhibit anomalous characteristics. Thus, for a simple redox reaction under diffusion control, the relationship between current (I) and time (t), is

$$I \propto t^{-n} \tag{10}$$

For a euclidean electrode surface n = 1/2, whereas for a fractal electrode surface the value of n depends on the fractal dimension D. A general expression relating n and D is

$$n = \frac{(D-1)}{2} \tag{11}$$

For the example of the electro-oxidation of the redox couple $[Fe(CN)_6]^{-4}/[Fe(CN)_6]^{-3}$ on gold under diffusion control, the log I *vs.* log t plot leads to n = 0.5 for a smooth electrode, and to n = 0.72 for a rough columnar electrode[28]. In this case, the value of n is consistent with $D_s = 2.44$ and $\alpha = 0.56$ for L_s values exceeding the average columnar size[24].

Isotropic disorder. Metallic dendrites

A dendritic deposit can be considered an isotropic strongly disordered system, its topography being very close to that resulting from the growth models involving diffusion limited aggregation (DLA) kinetics[29]. On the basis of fractal geometry, dendritic deposits exhibit a surface which can be described as a self-similar surface[6], whereas their volume or mass properties behave either as fractal or euclidean objects[30].

Characterization of dendritic surface electrodes

Self-similar objects can be characterized by different experimental methods. One of these methods consists of the determination of the mass of the object (M) and its gyration radius (R), the magnitudes of which maintain the proportionality,

$$M \propto R^{D_M} \tag{12}$$

where D_M is the mass fractal dimension. For metallic branched deposits, the value of M can be obtained from the electrodeposition charge, and the value of R by measuring high quality micrographs.

The surface properties of self-similar deposits with a euclidean mass ($D_M = 3$) can be obtained from the following relationship[6]:

$$A \propto V^{D_s/3} \tag{13}$$

where A, the area of the deposit, can be estimated from electroadsorption measurements, for instance, the underpotential electrodeposition charge of a metal, and V, from the value of Q related to the grown object.

A typical example of a branched system is a silver deposit (Fig. 9) grown in 10^{-3} M Ag_2SO_4 + 0.5 M Na_2SO_4 + 10^{-2} M H_2SO_4 at 25 °C[31,32].

The deposit growth remains isotropic until a certain critical radius (R_c) is reached. Then the anisotropic growth depends on the geometry of the electrochemical cell. Ac-

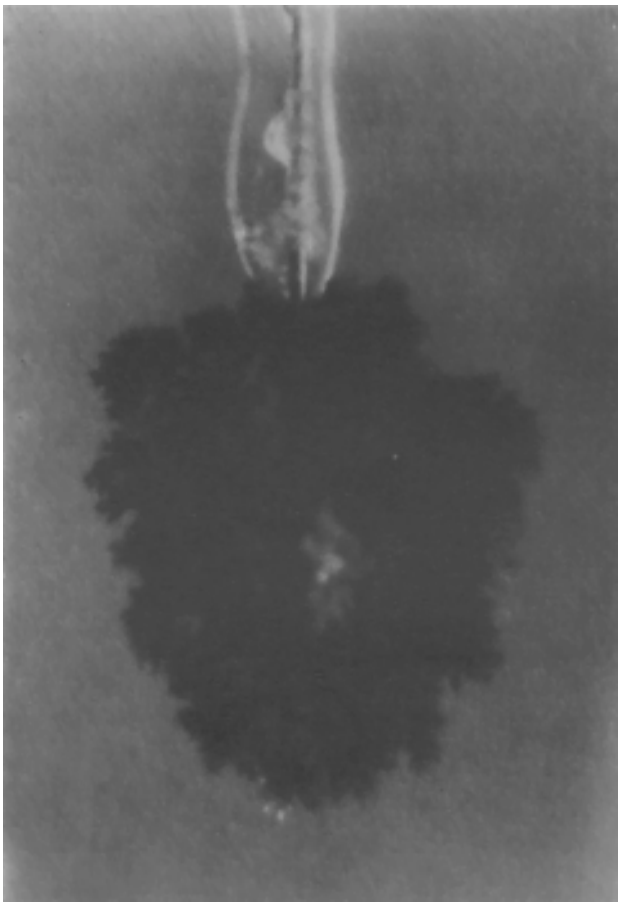

Figure 9. Branched silver deposit prepared on a silver cathode as indicated in the text.

cording to Eq. 12, the experimental data fit a log Q *vs.* log R plot with the slope equal to 3, as is necessary for a euclidean mass deposit. Likewise, for $R < R_c$, the slope of the log A *vs.* log Q plot (Eq. 13) results in $D_s = 2.5 \pm 0.03$ (Fig. 10). This figure coincides with the predictions of the DLA model[24]. These results demonstrate that in aqueous solution branched deposits exhibit a uniform density non-fractal mass, and a branched surface with fractal properties. Nevertheless, these characteristics depend considerably on the mass transport mechanism operating during object growth.

The influence of mass transport on the geometry of dendritic deposits

The influence of transport processes (migration, convection and diffusion) on branched electrodeposit growth can be studied by selecting adequate experimental conditions to enhance or to cancel one of the contributions already mentioned, and by changing the solution composition, the geometry of the cell, the hydrodynamic conditions and the potential routine applied to the system[33].

The convective effect which affects the growth and structure of the electrodeposit can be cancelled using a gel

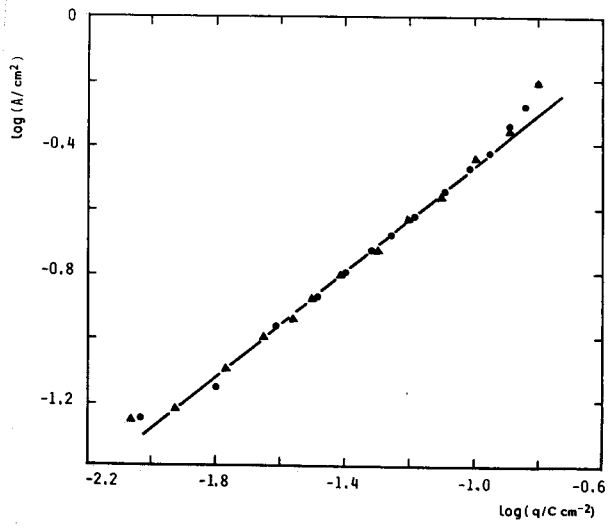

Figure 10. Plot of log A *vs.* log Q for branched silver deposits grown as indicated in the text. Deposit area determined by underpotential deposition of lead (•) and cadmium (▲). The linear plot remains unchanged in the range between the cathode size itself and R_c.

electrolyte[34]. Thus, for silver electrodeposition under the above-mentioned conditions, the addition of 0.5% agarose to the solution leads to a preferred isotropic growth of a deposit with values $D_s = D_M = 2.5$[34], as predicted by DLA models. From these experiments it can be concluded that the effect of convection on the deposit growth is to induce a macroscopic anisotropy during object growth, and an increase in its compactness, *i.e.* the object exhibits a euclidean mass.

Runs made in the gel imply the dominant contribution of migration and diffusion during the object growth. The contribution of migration itself can be enhanced by working in the absence of a supporting electrolyte Na_2SO_4. This leads to a dense branched deposit with non-fractal mass properties ($D_M = 3$)[35], whereas the deposit surface remains fractal ($D_s = 2.5$).

The preceding results can be represented by a Monte Carlo simulation of object growth[35] for two limiting situations. The first situation comprises a process in which particles moving at random are finally attached to the growing object. In this case $D_s = D_M = 2.5$, in agreement with DLA kinetic models. Therefore, the influence of the electric field on particle movement is negligible, a situation which is accomplished experimentally by adding a supporting electrolyte to the solution. The second situation arises when there is a biased particle shift towards the growing deposit, produced by the electric field. In this case $D_M = 3$ and $D_s = 2.5$. This is the case of those runs made in the absence of a supporting electrolyte in which the maximal influence of the electric field on the process can be attained. Consequently, as the migration contribution increases, the trend to produce denser non-fractal mass deposits is favored.

When real systems are considered, however, the description is usually more complex because there is a simultaneous, non-uniform contribution of migration and diffusion. Even in the solution containing a supporting electrolyte for an object growing with $D_S = D_M = 2.5$, its radial growth rate depends on the applied potential. The radius increases linearly with time instead of a linear $t^{2/3}$ dependence, as expected for DLA models[34,35]. This fact shows that the electric field dominates the growth velocity at branch tips, whereas the lateral growth is dominated by a local diffusion field.

Conclusions

Real single crystal metal surfaces at room temperature, columnar deposits and dendritic electrodeposits can be considered model systems for weakly and strongly anisotropic, and strongly isotropic disordered systems, respectively. Fractal geometry constitutes an important tool for the derivation of quantitative structural and kinetic information about the development of irregular surfaces which are of special interest in heterogeneous catalysis and electrocatalysis.

Acknowledgments

This paper is based upon data obtained from research projects which are financially supported by the Consejo Nacional de Investigaciones Científicas y Técnicas (CONICET) in Argentina.

References

1. G.I. Somorjai, *Chemistry in Two Dimensions: Surfaces* (Cornell University Press, Ithaca, 1981).
2. R.J. Bhem, *Scanning Tunnelling Microscopy and Related Methods* (R.J. Bhem, N. García and H. Rohrer, eds., Kluwer, 1990).
3. A.J. Arvia, R.C. Salvarezza and J.M. Vara, *Electrochim. Acta* **37**, 2155 (1992).
4. A.J. Arvia, J.C. Canullo, E. Custidiano, C. Perdriel and W.E. Triaca, *Electrochim. Acta* **31**, 1359 (1986).
5. P. Pfeifer and M. Obert, *The Fractal Approach to the Heterogeneous Chemistry* (Wiley, New York, 1989), p. 11.
6. B.B. Mandelbrot, *The Fractal Geometry of Nature*, (Freeman, New York, 1982).
7. D. Farin and D. Avnir, *The Fractal Approach to the Heterogeneous Chemistry* (D. Avnir, ed., Wiley, New York, 1989), p. 271. A. Seri-Levy and D. Avnir, *Langmuir* **9**, 3067 (1993); **9**, 3073 (1993).
8. F. Family, *Physica A* **168**, 561 (1990).
9. T. Vicsek, *Fractal Growth Phenomena* (World Scientific, Singapore, 1989).
10. F. Family and T. Vicsek, *J. Phys. A* **18**, L75 (1985).
11. R.C. Salvarezza, L. Vázquez, P. Herrasti, P. Ocón, J.M. Vara and A.J. Arvia, *Europhys. Lett.* **20**, 727 (1992).
12. R.F. Voss, *Fundamental Algorithms in Computer Graphics* (E.A. Earnshaw, ed., Springer Verlag, Berlin, 1985).
13. L. Vázquez, R.C. Salvarezza, P. Herrasti, P. Ocón, J.M. Vara and A.J. Arvia, *App. Surf. Sci.* **70-71**, 413 (1993).
14. P. Herrasti, P. Ocón., L. Vázquez, R.C. Salvarezza, J.M. Vara and A.J. Arvia, *Phys. Rev. A* **45**, 7440 (1992).
15. L. Vázquez, R.C. Salvarezza, P. Herrasti, P. Ocón, J.M. Vara and A.J. Arvia, submitted for publication.
16. D. Wolf and J. Villain, *Europhys. Lett.* **13**, 389 (1990).
17. Z.W. Lai and S. Das Sarma, *Phys. Rev. Lett.* **66**, 2348 (1991).
18. M. Kardar, G. Parisi and Y.C. Zhang, *Phys. Rev. Lett.* **56**, 889 (1986).
19. L. Vázquez, R.C. Salvarezza, P. Ocón, P. Herrrasti, J.M. Vara and A.J. Arvia, *Phys. Rev. E.* **49**, 1507 (1994).
20. P. Herrasti, P. Ocón, L. Vázquez, R.C. Salvarezza, J.M. Vara and A.J. Arvia, *J. Phys. Chem.* **98**, 2418 (1994).
21. J.M. Morales, P. Esparza, S. González, L. Vazquez, R.C. Salvarezza and A.J. Arvia, in preparation.
22. J.L. Zubimendi, M.E. Vela, R.C. Salvarezza, L. Vázquez, J.M. Vara and A.J. Arvia, *Langmuir*, in press.
23. J.L. Zubimendi, M.E. Vela, R.C. Salvarezza, L. Vázquez, J.M. Vara and A.J. Arvia, *Phys. Rev. E.* **50**, 1367 (1994).
24. J.M. Gómez-Rodríguez, L. Vázquez, A. Baró, R.C. Salvarezza, J.M. Vara and A.J. Arvia, *J. Phys. Chem.* **96**, 347 (1992)
25. R. de Levie, *Electrochim. Acta* **9**, 1231 (1964).
26. T. Pajkossi, *J. Electroanal. Chem.* **300**, 1 (1991).
27. M. Gómez, L. Vázquez, R.C. Salvarezza, J.M. Vara and A.J. Arvia, *J. Electroanal. Chem.* **317**, 125 (1991).
28. P. Ocón, P. Herrasti, L. Vázquez, R.C. Salvarezza, J.M. Vara and A.J. Arvia, *J. Electroanal. Chem.* **319**, 101 (1991).
29. T.A. Witten and L.M. Sander, *Phys. Rev. Lett.* **47**, 1400 (1981).
30. P. Meakin, *The Fractal Approach to the Heterogeneous Chemistry* (Wiley, New York, 1989), p. 131.
31. A. Hernández-Creus, P. Carro, S. González, R.C. Salvarezza and A.J. Arvia, *J. Electrochem. Soc.* **139**, 1064 (1992).
32. A. Hernández-Creus, A.E. Bolzan, P. Carro, S. González, R.C. Salvarezza, S.L. Marchiano and A.J. Arvia, *J. Electroanal. Chem.* **336**, 85 (1992).
33. V. Levich, *Physicochemical Hydrodynamics* (Prentice-Hall, Englewood Cliffs, 1962).
34. P. Carro, A. Hernández-Creus, S. González, R.C. Salvarezza, S.L. Marchiano and A.J. Arvia, *Phys. Rev. E.* **48**, R2374 (1993).
35. A. Hernández-Creus, P. Carro, S. González, R.C. Salvarezza, S.L. Marchiano and A.J. Arvia, *Fractals in Natural and Applied Sciences* **A-41**, 191 (1994).